Supporting Information

Satterthwaite et al. 10.1073/pnas.1400178111

SI Methods

Participants. Overall, 1,445 subjects were enrolled. However, 273 were excluded from the current analysis sample owing to clinical factors including medical disorders that could affect brain function ($n = 51$), current use of psychoactive medications ($n = 168$), prior inpatient psychiatric treatment ($n = 51$), or an incidentally encountered structural brain abnormality ($n = 18$); subjects frequently met more than one exclusionary criterion. An additional 14 subjects were excluded for missing data. Among the 1,158 eligible for inclusion, 113 subjects were imaged with at least one sequence (e.g., T1-weighted imaging) but did not complete either the arterial spin labeling or field map sequences. Of the 1,045 subjects who had complete data and were not excluded owing to clinical criteria, 123 were excluded as part of imaging quality assurance, including excessive motion (mean relative displacement >0.5 mm), low temporal signal-to-noise ratio (tSNR <30), poor image coverage, or an excessive number of voxels that had ceiling intensity values at some point in the timeseries (>500; discussed below). This yielded a final sample of 922 subjects included in the present report.

Assessment of Secondary Sex Characteristics. Following general instructions, participants privately viewed pictorial representations, accompanied by text descriptions, of the five Tanner stages of pubic hair growth appropriate for their sex and rated their own development on the scale from 1 to 5 (1). Prior validation studies have compared such self-report procedures with Tanner staging conducted by a physician and found that correlations between physician ratings and self-reported pubic hair ratings were 0.81 for girls and 0.63 for boys (2).

Grouping of Pubertal Stages. As noted above, pubertal assessment was only available for subjects over the age of 10. As a result, the number of pre/early-pubertal subjects was relatively small. Accordingly, we grouped Tanner stages 1–3 into a prepubertal bin to ensure that the sample size of that bin would be more comparable to the samples within the larger midpubertal (Tanner stage 4) and postpubertal (Tanner stage 5) bins. The number of male and female subjects for each Tanner stage before grouping is provided in Table S1. Notably, results of analyses of the effect of puberty were the same when raw (ungrouped) Tanner stages were used: There was no sex difference within the Tanner stages that were grouped to make the prepubertal bin (e.g., Tanner stages 1–3). Results from Tanner stage 4 (midpubertal) and Tanner stage 5 (postpubertal) were unchanged because they were not grouped in the main analysis.

Image Acquisition. As previously described (3), all subject data were acquired on the same scanner (Siemens TIM Trio 3 Tesla; 32 channel head coil) using the same imaging sequences. Brain perfusion was imaged using a custom pseudocontinuous arterial spin labeling (pCASL) sequence (4). The sequence used a single-shot spin-echo echo-planar imaging readout. The arterial spin labeling parameters were TR 4 s, TE 15 ms, flip angle 90/180°, FOV 220 × 220 mm, matrix 96 × 96 × 20, slice thickness/gap 5/1 mm, effective voxel resolution 2.3 × 2.3 × 6 mm, label duration 1,500 ms, postlabel delay 1,200 ms, GRAPPA 2, 80 volumes (40 label, 40 control), and total acquisition time 5:32 min. The slices were acquired in ascending, noninterleaved order to avoid slice ordering confounds associated with interleaved schemes. To ensure that all slices had a similar postlabel delay, slices were acquired in a compressed scheme immediately following the postlabel delay, rather than distributing the slice acquisitions evenly throughout the TR period.

Before the pCASL sequence, a magnetization-prepared, rapid acquisition gradient-echo T1-weighted image was acquired to aid spatial normalization to standard atlas space, using the following parameters: TR 1,810 ms, TE 3.51 ms, TI 1,100 ms, FOV 180 × 240 mm, matrix 192 × 256, 160 slices, slice thickness/gap 1 mm/0 mm, flip angle 9°, GRAPPA 2, effective voxel resolution of 0.9 × 0.9 × 1 mm, and total acquisition time 3:28 min. Additionally, a B0 field map was acquired for application of distortion correction procedures, using a double-echo gradient recall echo sequence: TR 1,000 ms, TE1 2.69 ms, TE2 5.27 ms, 44 slices, slice thickness/gap 4 mm/0 mm, flip angle 60°, FOV = 240 mm, effective voxel resolution of 3.8 × 3.8 × 4 mm, and total acquisition time 1:04 min.

Image Preprocessing. All imaging data were loaded into an XNAT database (5) that included custom front-end (QLUX) software that monitored quality assurance by checking that acquisition parameters matched a study-defined template. Basic preprocessing of the perfusion images was completed using tools that are part of FSL (6). Images were distortion-corrected using FUGUE, motion-corrected using MCFLIRT (7), and spatially smoothed (6 mm FWHM). The last four image pairs of the series were discarded, which we have observed to substantially reduce a frequency-dependent lipid artifact in the present spin-echo pCASL data.

Cerebral Blood Flow Quantification. Because prior work has shown that the T1 relaxation time changes substantially in development and varies by sex, this parameter was set according to the methods outlined in Wu et al. (8). Prior validation studies have shown that this procedure enhances accuracy and reliability in pediatric populations (9). A potential limitation of this work is the assumption that arterial blood T1 can be calculated using the model derived by Wu et al. (8). That work derived an expression for venous blood T1 as a function of age and sex. An alternative approach would involve measuring blood T1 independently in each subject, which is challenging and time-consuming to measure in vivo. Moreover, the work of Jain et al. (9) demonstrated that empirically measured blood T1 introduced greater test–retest variability compared with relying on a T1 model. Another aspect of this approach that merits further consideration is the reliability of using a venous blood T1 model for the estimate of arterial blood T1. Notably, arterial and venous T1 are similar (within 100 ms at 3 T), and both blood pools show very little dependence over the physiologic range of hemoglobin saturation. Furthermore, both arterial and venous blood T1 follow a similar dependence on hematocrit level (10), supporting the assumption of a similar dependence on age- and sex-related changes in blood chemistry.

Image Registration. Subject-level cerebral blood flow (CBF) maps were coregistered to the T1 image using boundary-based registration (11) with integrated distortion correction as implemented with tools that are part of FSL (6). Whole-head T1 images were registered to the Montreal Neurologic Institute (MNI) 1-mm template via the top-performing symmetric normalization methodology available in Advanced Normalization Tools (12–14). Images were down-sampled to 2-mm resolution before group-level analysis. All registrations were inspected manually and also evaluated for accuracy using spatial correlations. Subject-space CBF maps were registered to the template by concatenating transformations from

coregistration, distortion correction, normalization, and downsampling, so that only one interpolation was performed in the entire process.

Group-Level Analyses Covariates. Covariates included in the general additive model race, in-scanner motion, and gray matter density (calculated on a voxelwise basis). Race was categorized as Caucasian or African–American, modeled in separate regressors versus a baseline of other (neither Caucasian nor African–American). As in our prior work on motion artifact in resting-state functional connectivity data, motion was summarized as the mean relative rms displacement estimated by time-series realignment (15). Because CBF is higher in gray matter than white matter, differences in brain structure could potentially confound analyses of brain perfusion (16). Accordingly, gray matter density was calculated from the T1 image segmentation using Atropos (17) and modeled on a voxelwise basis. Finally, in this dataset voxel intensity values occasionally reflected the maximum digitization reported by the scanner, suggesting that these values had been clipped at a ceiling intensity value. As noted above, subjects with >500 voxels with ceiling intensity values at any point in the time-series acquisition were excluded from analysis; in the remaining subjects on average only 1.18% of voxels per subject were affected. However, to be conservative, this effect was modeled on a voxelwise basis for each subject at the group level using a binary regressor, effectively censoring the influence of such voxels within the group level analysis. Thus, at each voxel the GAM used was

$$\begin{aligned}\mathrm{CBF} = {} & \mathrm{intercept} + \mathrm{sex} + \mathrm{spline(age\ by\ sex)} + \\ & \mathrm{race_{cauc}} + \mathrm{race_{af-am}} + \mathrm{motion} + \mathrm{GMD_{vox}} + \mathrm{ceiling_{vox}}.\end{aligned}$$

This GAM was run on 109,748 gray matter voxels (as defined by the MNI template).

1. Tanner JM (1971) Sequence, tempo, and individual variation in the growth and development of boys and girls aged twelve to sixteen. *Daedalus* 100:907–930.
2. Morris NM, Udry JR (1980) Validation of a self-administered instrument to assess stage of adolescent development. *J Youth Adolesc* 9(3):271–280.
3. Satterthwaite TD, et al. (2014) Neuroimaging of the Philadelphia neurodevelopmental cohort. *Neuroimage* 86:544–553.
4. Wu W-C, Fernández-Seara M, Detre JA, Wehrli FW, Wang J (2007) A theoretical and experimental investigation of the tagging efficiency of pseudocontinuous arterial spin labeling. *Magn Reson Med* 58(5):1020–1027.
5. Marcus DS, Olsen TR, Ramaratnam M, Buckner RL (2007) The Extensible Neuroimaging Archive Toolkit: An informatics platform for managing, exploring, and sharing neuroimaging data. *Neuroinformatics* 5(1):11–34.
6. Jenkinson M, Beckmann CF, Behrens TEJ, Woolrich MW, Smith SM (2012) FSL. *Neuroimage* 62(2):782–790.
7. Jenkinson M, Bannister P, Brady M, Smith S (2002) Improved optimization for the robust and accurate linear registration and motion correction of brain images. *Neuroimage* 17(2):825–841.
8. Wu W-C, et al. (2010) In vivo venous blood T1 measurement using inversion recovery true-FISP in children and adults. *Magn Reson Med* 64(4):1140–1147.
9. Jain V, et al. (2012) Longitudinal reproducibility and accuracy of pseudo-continuous arterial spin-labeled perfusion MR imaging in typically developing children. *Radiology* 263(2):527–536.
10. Lu H, Clingman C, Golay X, van Zijl PCM (2004) Determining the longitudinal relaxation time (T1) of blood at 3.0 Tesla. *Magn Reson Med* 52(3):679–682.
11. Greve DN, Fischl B (2009) Accurate and robust brain image alignment using boundary-based registration. *Neuroimage* 48(1):63–72.
12. Avants BB, Epstein CL, Grossman M, Gee JC (2008) Symmetric diffeomorphic image registration with cross-correlation: Evaluating automated labeling of elderly and neurodegenerative brain. *Med Image Anal* 12(1):26–41.
13. Avants BB, et al. (2011) A reproducible evaluation of ANTs similarity metric performance in brain image registration. *Neuroimage* 54(3):2033–2044.
14. Klein A, et al. (2009) Evaluation of 14 nonlinear deformation algorithms applied to human brain MRI registration. *Neuroimage* 46(3):786–802.
15. Satterthwaite TD, et al. (2013) Heterogeneous impact of motion on fundamental patterns of developmental changes in functional connectivity during youth. *Neuroimage* 83:45–57.
16. Taki Y, et al. (2011) Correlation between gray matter density-adjusted brain perfusion and age using brain MR images of 202 healthy children. *Hum Brain Mapp* 32(11): 1973–1985.
17. Avants BB, Tustison NJ, Wu J, Cook PA, Gee JC (2011) An open source multivariate framework for n-tissue segmentation with evaluation on public data. *Neuroinformatics* 9(4):381–400.

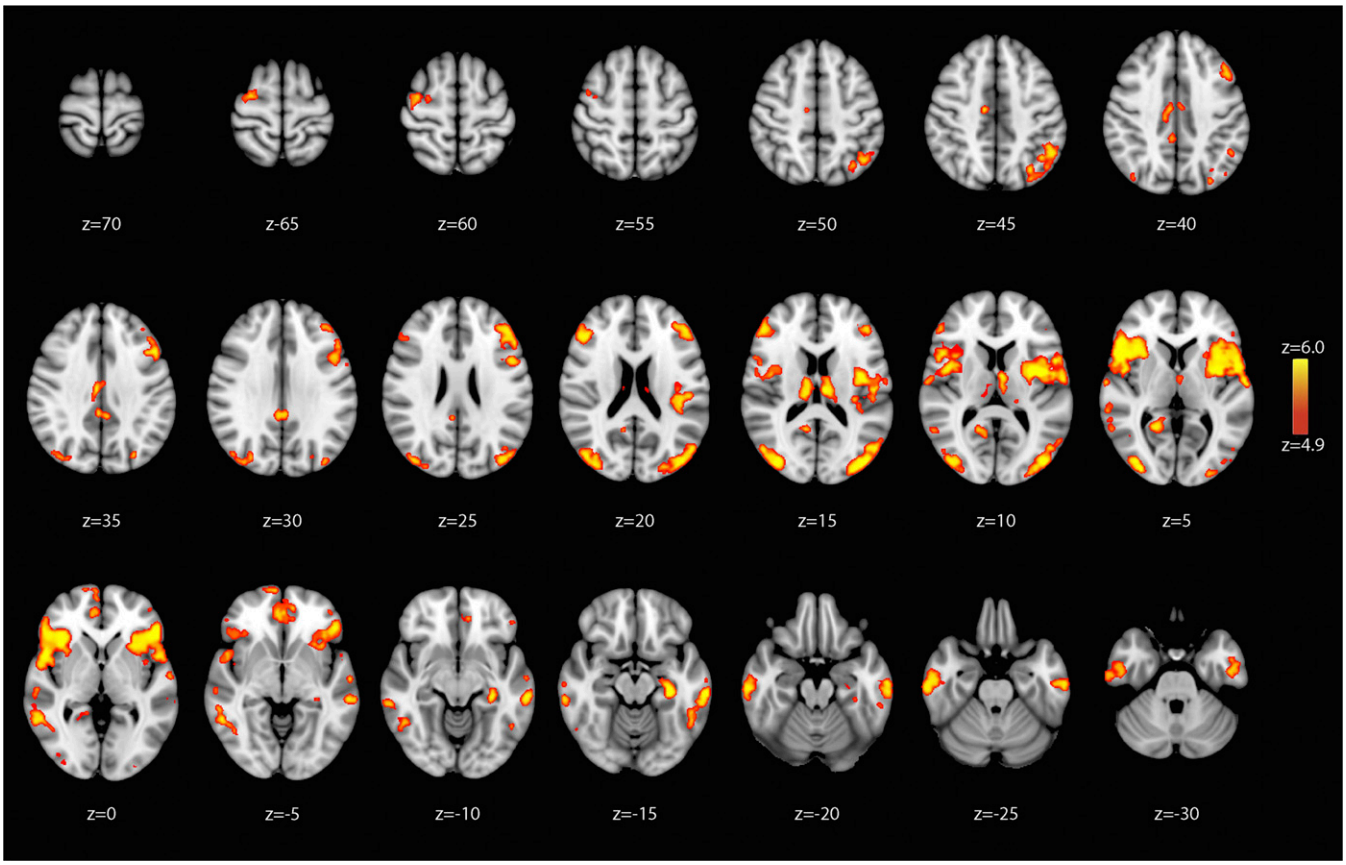

Fig. S1. Complete voxelwise results of nonlinear age-by-sex interaction in sample of 922 subjects.

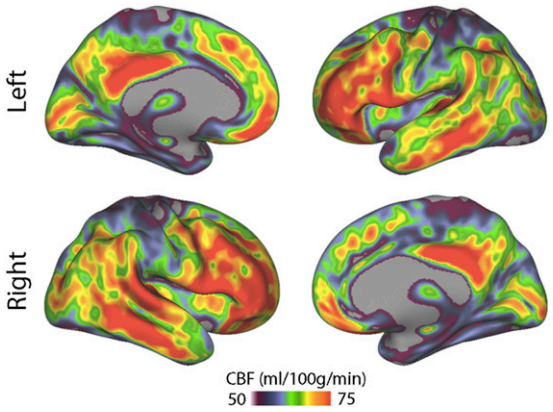

Fig. S2. Mean CBF across complete sample of 922 subjects.

Table S1. Sample by ungrouped pubertal stage (n = 769)

Pubertal stage	No. female	No. male
Tanner 1	18	22
Tanner 2	39	30
Tanner 3	36	46
Tanner 4	109	109
Tanner 5	225	115